Since January 2020 Elsevier has created a COVID-19 resource centre with free information in English and Mandarin on the novel coronavirus COVID-19. The COVID-19 resource centre is hosted on Elsevier Connect, the company's public news and information website.

Colloid and Interface Science Communications 40 (2021) 100356

Contents lists available at ScienceDirect

Colloid and Interface Science Communications

journal homepage: www.elsevier.com/locate/colcom

Rapid Communication

Spectroscopic investigation on the affinity of SARS-CoV-2 spike protein to gold nano-particles

Kazushige Yokoyama *, Akane Ichiki

Department of Chemistry, The State University of New York Geneseo College, 1 College Cir., Geneseo, NY 14454, USA

ARTICLE INFO

Keywords:
SARS-CoV-2
Spike protein
Gold nano-colloidal particles
Protein folding
Reversible self-assembly

ABSTRACT

The affinity of the SARS-CoV-2 spike protein (S protein) to gold nano-particles was examined through spectral shifts of SPR (Surface Plasmon Resonance) band. Gold nano-colloidal particles are sensitive to the conformational change of the protein adsorbed over the particles' surface. As the pH value was gradually lowered from approximately neutral pH to an acidic pH (*ca.* pH 2), all mixtures of S protein with the gold colloids ≥30 nm in diameter exhibited a drastic red-shift of the average SPR band peak at one pH value more than that observed for bare gold colloids. The surface coverage fraction (Θ) of S protein over the nano-particle's surface was extracted and all showed relatively small coverage values (*i.e.,* Θ ~ 0.30). The SPR band peak shift was also examined as the pH values were hopped between pH ~ 3 and pH ~ 10 (pH hopping). As the pH values hopped, an alternation of the average SPR band peaks were observed. A significant amplitude of an alternation was especially observed for the mixture of S protein with gold ≥30 nm of gold size implying the reproduction of pH induced reversible protein folding. We hypothesize that the pH hopping scheme captured a reversible transition between folded or Down conformation (pH ≥ ~7) and unfolded or Up (pH ~ 3) conformation of RBD (receptor binding domain). The acidic condition may also dimerize the S protein through RBD. The Up conformation or dimerization of S protein are considered to be connected to the other gold nano particles forming gold nano-particle aggregates.

A number of pathogenic viruses, including Chikungunya virus, Dengue virus, HIV (Human Immunodeficiency Virus), Influenza virus, Zaire Ebola virus, SARS-CoV, MERS-CoV, and SARS-CoV-2, are protected by a viral membrane which requires this viral capsid to fuse with a cell as an initial step in the infection process [1]. This fusion process utilizes glycoproteins on the surface of the viral membrane to interact with cell surface proteins to help catalyze membrane fusion [2]. Extensive studies have been accumulating on the SARS-CoV-2 infection process (virus which causes COVID-19). The cell fusion process is initiated and completed by a spike protein (S protein), which is a trimeric class I viral fusion protein. After the receptor binding domain (RBD) [3–7] of the viral S protein attaches to ACE2 (Angiotensin Converting Enzyme) receptors on the cell surface [7–14], where the initial cleavage of the S protein is assumed to be triggered as pH decreases during endocytosis. Cleavage separates the trimers' S1 domain (top head) at the N-terminus side of the protein from the S2 domain which includes the viral transmembrane motif. Subsequent cleavage by TMPRSS2 (Transmembrane protease serine 2) removes the S2′ N-terminal region from the remainder of the S2 domain (which still contains the transmembrane motif), which causes the unfolding of the fusion protein resulting in a formation of extended fusion protein intermediates and allowing the access to the target (cell) membrane [15]. Finally, under around pH 4 condition, the extended fusion proteins fold-back [16] in order to make two membrane surfaces come closer to reach a hemifusion stage, followed by a completion of the membrane fusion process [17–21] and releasing RNA containing viral information into the cell cytoplasm. An initiation of a viral infection is summarized as a completion of a cell-fusion through energetically unfavorable "folding back" conformational change by the extended fusion protein intermediates. Thus, design of inhibitor drug development may effectively proceed by targeting the characterization of S protein segment [22–27]. If a nano-particle functionalized with S protein can provide a spectroscopic signal on its property change, this can be utilized for an evaluation of an inhibitor and speeding up the screening process in identifying the strong candidate drug.

In this work we investigated whether the gold nano-particles possess adequate affinity to anchor the S protein [28,29]. In our previous work, the orientation of the amyloidogenic peptide over the nano-gold surface

* Corresponding author.
E-mail addresses: yokoyama@geneseo.edu (K. Yokoyama), ai7@geneseo.edu (A. Ichiki).

https://doi.org/10.1016/j.colcom.2020.100356
Received 2 November 2020; Received in revised form 15 December 2020; Accepted 20 December 2020
Available online 26 December 2020

was found to take a "spiking-out" orientation in order to maximize the possibility of the networking [30,31]. Under low pH (less than pH 4), the amyloidogenic peptides conduct protein unfolding and complete the networking to the other peptide over the other surrounding gold colloid. This results in the formation of gold colloid aggregates. This orientation was consistent with the study revealed on bi-polymer over metal nano particles. The orientation observed in amyloidogenic peptides is similar to that of S protein contained on a viral membrane. Also, the possible reversible self-assembly was observed with amyloidogenic peptides over the nano-gold surface [32]. There has been a great effort of dealing with SARS-CoV-2 utilizing the nanotechnology [33–40], and we hypothesize that we can reproduce the functionality of the S protein over the nano-gold surface to investigate the kinetics path of S protein in the fusion process. Sekimukai and et al. attempted to create S protein complex by using 40 nm and 100 nm gold nano-particles as platforms. It was reported to induce a strong *IgG* response but failed to improve vaccine efficacy or to reduce eosinophilic infiltration because of highly allergic inflammatory responses. The current work examine the affinity of S protein to various sizes of nano-particles at more simplified environment, *i.e.,* aqueous condition at *ca.* 25 °C. A model system of the S protein would further the field's understanding of the SARS-CoV-2 protein itself, potentially aiding in the design or discovery of drugs or of inhibitors and serving as an *in vitro* screening tool for drug screening [41].

The SARS-CoV-2 (COVID-19) S protein (R683A, R685A) His Tag (138 kDa) was purchased from ACRO Biosystems (Newark, Delaware, USA). The active trimer (SPN-C52H8) was expressed from human 293 cells (HEK293) and it contains AA Val 16-Pro 1213 trimer design. The predicted N-terminus is [16]Val. The purity was reported to be 96.90% as determined by HP-SEC and 556.40 kDa verified by MALS. Under room temperature, 250 μL of distilled deionized water (~18 MΩ and purified by Milli-Q-water system (Millipore) was added to 50 μg of S protein to make the stock solution of S protein with 1.45 μM and stored in a − 80 °C freezer.

As described in the previous work [31], nine different sizes of gold colloidal particles (diameter d = 10, 15, 20, 30, 40, 50, 60, 80, and 100 nm) purchased from Ted Pella Inc. (Redding, California, USA) The residual stabilizer contained in all sizes of gold colloids were negligible (*e.g.*, citrate $<10^{-5}$%, tannic acid $<10^{-7}$% and potassium carbonate $<10^{-8}$%) [12] The reported values of the estimated diameters (d), measured diameter (*d*), and particles per mL for each gold colloid are shown in Table 1b. The concentration of S protein was fixed as 360 pmol [31], and the ratio of [S protein] / [Gold Colloid] as 4, 19, 39, 136, 303, 665, 1269, 2479, and 3409 for the 10, 15, 20, 30, 40, 50, 60, 80, and 100 nm gold colloid, respectively. The attachment of protein to the gold colloidal surface was expected to be achieved almost instantaneously and considered to reach equilibrium within a minute. The UV–Vis absorption spectra were monitored between 400 and 1200 nm. There were two schemes to examine the peak shift of SPR (Surface Plasmon Resonance) band of gold nanoparticles residing around *ca.* 530 nm at pH 7. The first scheme is to monitor the SPR peak as a function of a gradual change of pH to the acidic condition up to pH 2 by externally adding 0.100 M HCl (hydrochloric acid) with roughly 4 min interval (two minute for equilibrating the mixture and two minutes of data collection time) and the step of 0.2 pH, *pH step-wise change scheme*. Another scheme was to observe SPR band peak shift as pH was hopped between acidic at pH 3.1 ± 0.6 and basic condition around pH 9.7 ± 0.5, *pH hopping scheme*. Each spectrum at a given pH point (operation number, n) was obtained within five minutes while the system was under dynamic equilibrium. The pH ($n = 1$) was around pH 7 (*i.e.*, pH (initial) listed in Table 1a), then pH was shifted to pH 3.1 ± 0.6 for an even n, and to pH = 9.75 ± 0.5 for an odd n. All data collections in both schemes were conducted under 24.5 ± 0.2 °C. Each pH value at each operation number, n, was gained without fine adjusting the pH values in order to make the duration time (300 ± 10 s) for each operation number to be equal and to maintain kinetic condition the same.

Table 1
The optimized parameters for the sigmoidal curve of $\overline{\lambda_{peak}}$ *vs.* pH using the Boltzmann model shown in Eq. (2) for a) mixture of S protein and gold nanoparticle of size d and b) for bare gold colloids [31] at 24.5 ± 0.2 °C. (d: reported diameter, N: number of particles) c) The difference of pH_o between pH_o of S protein-gold mixture and that of bare gold, ΔpH_o. The standard deviation of the last digit is given in the parenthesis, ().

a)	d (nm)	λ_{max} (nm)	λ_{min} (nm)	pH_o	*d*pH	$<R^2>$	pH (initial)
	10	630(2)	585.4 (5)	3.27 (2)	0.21 (2)	0.9799	6.302
	15	650(2)	582.4 (7)	3.54 (3)	0.31 (2)	0.9902	6.378
	20	643(2)	585.2 (5)	3.33 (4)	0.37 (3)	0.9900	6.737
	30	644(2)	569.8 (9)	4.34 (2)	0.20 (2)	0.9888	6.917
	40	663(1)	574(1)	4.32 (2)	0.22 (2)	0.9944	7.069
	50	651(2)	567(2)	4.28 (1)	0.092 (1)	0.9803	7.136
	60	668(3)	562(2)	4.180 (7)	0.051 (8)	0.9815	7.355
	80	684(1)	571.5 (7)	4.47 (1)	0.26 (1)	0.9978	7.392
	100	698.5 (9)	617.2 (9)	4.85 (2)	0.26 (2)	0.9950	6.985
	Average	660 (22)	580 (16)	4.1(5)	0.22 (9)	0.989 (6)	4.1(6)

b)	d (nm)	*d* (nm)	N (particles mL^{-1})	λ_{max} (nm)	λ_{min} (nm)	pH_o	*d*pH
	10	9.8 ± 1.0	1.4×10^{12}	564 (5)	517 (3)	3.4(1)	0.2(1)
	15	15.2 ± 1.5	2.8×10^{11}	578 (2)	523.3 (2)	3.07 (5)	0.34 (2)
	20	19.7 ± 1.1	1.4×10^{11}	615 (6)	526 (4)	3.70 (7)	0.24 (2)
	30	30.7 ± 1.3	4.0×10^{10}	597 (1)	574.7 (5)	4.05 (5)	0.32 (4)
	40	40.6 ± 1.1	1.8×10^{10}	661 (2)	528 (1)	4.32 (7)	0.11 (1)
	50	51.5 ± 4	8.2×10^{9}	700 (4)	533 (2)	4.06 (2)	0.11 (1)
	60	60 ± 1.0	4.3×10^{9}	691 (4)	535 (2)	4.21 (1)	0.11 (1)
	80	80 ± 1.0	2.2×10^{9}	709 (2)	571 (1)	4.246 (4)	0.060 (4)
	100	99.5 ± 1.3	1.6×10^{9}	708 (2)	598.9 (7)	3.950 (4)	0.057 (4)
	Average	–	–	650 (59)	550 (29)	3.9(4)	0.2(1)

c)	d (nm)	ΔpH_o
	10	−0.13
	15	0.47
	20	−0.37
	30	0.29
	40	0.01
	50	0.22
	60	−0.03
	80	0.224
	100	0.9
	Average	0.2 (4)

Under the step-wise pH change scheme, the gradual red shift of SPR band was observed as shown in Fig. 1, where for S protein mixed with 50 nm gold colloid particles as a representative example. The average peak band position ($\overline{\lambda_{peak}}$) was extracted by selecting the region between 450 nm and 850 nm, which exhibit the sensitive response as the pH condition alters [32]. The $\overline{\lambda_{peak}}$ of each pH condition was obtained by Eq. (1).

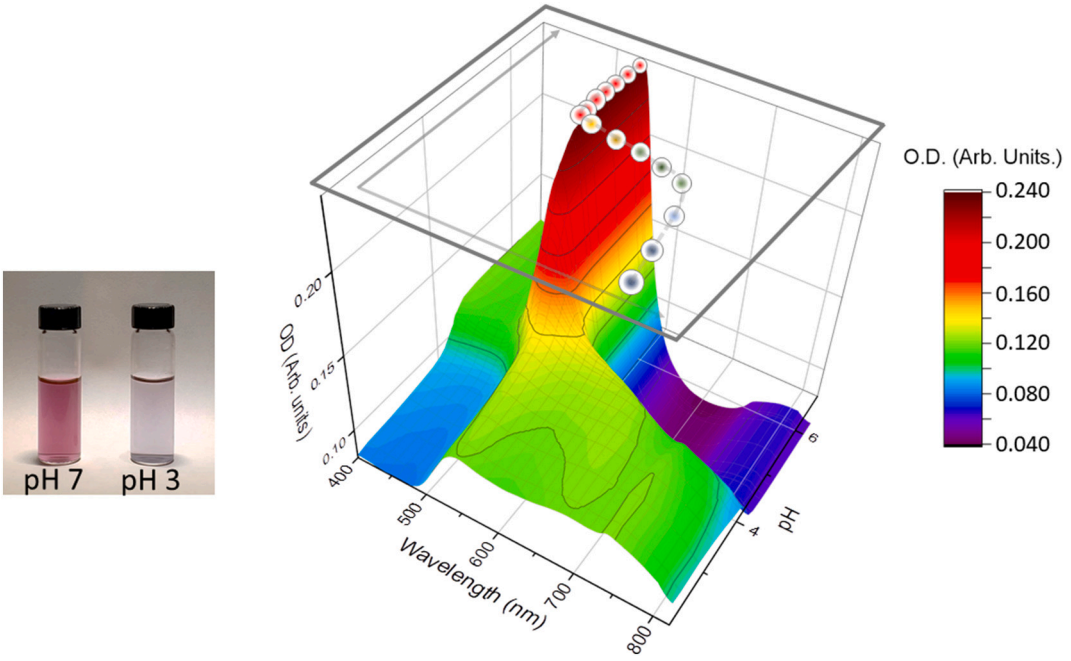

Fig. 1. The SPR band shift for 50 nm gold colloid coated with S protein (at 25 °C). In order to illustrate the mixture condition, the inset picture demonstrates the color of the mixture at pH ~7 (or pH ~10) and that at pH ~3 with roughly 10 times higher concentration than was used for the SPR study. (For interpretation of the references to color in this figure legend, the reader is referred to the web version of this article.)

$$\overline{\lambda_{peak}} = \sum_{i=1}^{m} a_i\lambda_i \Big/ \sum_{i=1}^{m} a_i \tag{1}$$

here, λ_i is the central peak position of *i*th component of the band and a_i is the area of the *i*th component of the band expressed by a Gaussian profile. Both λ_i and a_i were extracted by Peak Fit function of OriginPro 2018b (Origin Lab). For an entire processes, the maximum peak component values, m, was limited to 3 and the optimum fit was achieved with average R-squared, $<R^2>$, of 0.995(2). Each $\overline{\lambda_{peak}}$ at a given pH was depicted and formed a sigmoidal curve and shown as a sketch on the top part in Fig. 1 as a projected plot. The sigmoidal curves were fit by the Boltzmann model given in Eq. (2).

$$\overline{\lambda_{peak}}\,(pH) = \frac{\lambda_{min} - \lambda_{max}}{\left\{1 + e^{\left[pH - pH_o\right]/dpH}\right\}} + \lambda_{max} \tag{2}$$

here, the λ_{min} and λ_{max} stand for the minimum and maximum of the band peak positions, respectively. The most important piece of information from this analysis is the pH_o, which shows the pH where color change takes place with the first derivative of the λ_{peak}(pH), λ_{peak} [1]. The value *d*pH shown in Eq. (2) was expressed as $d\text{pH} = (\lambda_{max} - \lambda_{min})/4\lambda_{peak}$ [1]. The sigmoidal curves for d = 10 nm and 100 nm are shown in Fig. 2 as two representative sigmoidal curves and exhibiting the trend generally observed in this study. As a comparative guide, the pH_o for bare gold colloid of 10 nm and 100 nm are shown as (a)′ and (b)′ in Fig. 2. The optimized parameters for sigmoidal curves with Eq. (2) are tabulated in Table 1a and in Table 1b for S protein gold mixture and for bare gold [30], respectively. The pH_o was around 3.0 for the mixture with the gold nano-particles of d ≤ 20 nm, while it was over pH 4 for d ≥ 30 nm (Table 1a), and this was the basic trend also observed in bare gold colloids (Table 1b). In order to seek for an indication of the surface property change, the difference of pH_o between S protein/gold nano-particle mixture and bare gold colloid (ΔpH_o) was shown at Table 1c.

The surface property change due to the protein coverage can be detected by the ΔpH_o. However, there was no significant trend observed in the ΔpH_o with respect to the colloidal size. The largest difference was found in 100 nm gold colloid, and no significant differences were found for 40 nm and 60 nm gold. Based on the same technique with amyloidogenic peptide coated gold nano-particles [31], all tested nano-size gold colloid showed the positive ΔpH_o and indicates that peptides were coated. However, under the current study, several gold colloids exhibited negative ΔpH_o, implying that the S protein coating over the nano-gold colloid with δ– segment requiring extra addition of H_3O^+, more than what bare gold colloids need. Thus, $|\Delta pH_o|$ can be used as the indicative of the surface character change, the same analysis of the *d*pH *vs.* $|\Delta pH_o|$ conducted for amyloidogenic peptides [30,31]. However, the trend of *d*pH with the S protein was opposite to what was observed in

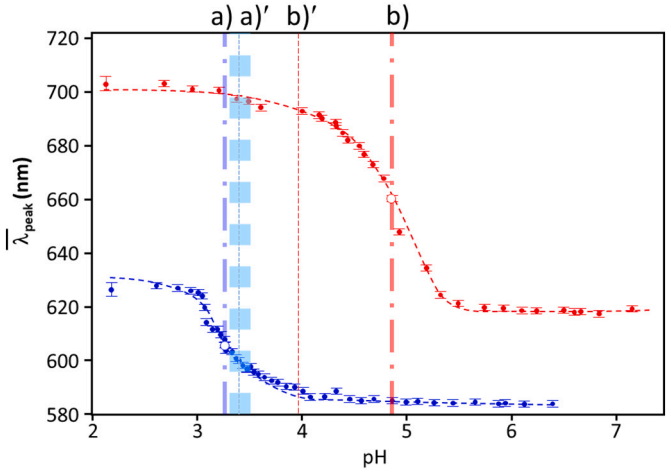

Fig. 2. Typical sigmoidal fits. Examples for gold 10 nm (blue) and 100 nm (red) are shown. The pH a) and b) show the values at where the color change (*i.e.*, colloidal aggregation) takes place. The pH at a)′ and b)′ are for the bare gold with the width of the standard deviation of each pH_o. The width of vertical lines correspond to the standard deviations of each pH_o. (For interpretation of the references to color in this figure legend, the reader is referred to the web version of this article.)

amyloidogenic peptides. The analysis was re-conducted with $1/d\mathrm{pH}$ *vs.* $|\Delta \mathrm{pH_o}|$ model and satisfactory fit was achieved [42]. The average coverage fraction (Θ) was relatively low (*ca.* 0.30) compared to those observed for amyloidogenic peptides (Θ_{avg} [$A\beta_{1\text{-}40}$] = 0.6 ± 0.2, Θ_{avg} [α-syn.] = 0.5 ± 0.2, and Θ_{avg} [β2m] = 0.7 ± 0.2) [30]. The highest Θ[S protein] was 0.90 for d = 100 nm gold nano particles, and d = 40 and 60 nm exhibited Θ = 0. The geometrical shape of S protein is consisting of a globular head and a stalk though, initial optimization geometry was conducted with prolate top and $a = 5.3$ and $b = 8.9$ nm were used based on the reported crystal structure [43], since occupying area is projected as the circle limited by of a globular head, which can be replaced with a circle projected from the prolate top as well. No conclusive evidence was obtained for the orientation of the S protein over the gold colloidal surface as to whether it adsorbs with a lying-down orientation or spiking-out orientation. While the geometrical analysis of the adsorption and the Θ is not a focus of this paper and will be reported in the future [42], the optimized geometrical values for a simplified prolate models showed significant nano-size dependence. For most of the gold sizes relatively low Θ are explained by gyration motion of S protein with spiking-out orientation. The high Θ observed in the 100 nm was concluded due to the relatively high contribution, ~50%, of the 2nd layer (*i.e.,* insertions of the S protein adsorbed on the other surrounding gold nano-particles). The negligible Θ in d = 40 nm and 60 nm was explained by employing an empirical factor indicating that the adsorbed S proteins did not impact $\Delta \mathrm{pH_o}$ [42]. Here, it should be noted that in our geometrical simulation model the number of adsorption spots is as an index of the surface coverage. Therefore, the explanation above using the occupations by extended long chain proteins may explain the smaller adsorption spots.

The sigmoidal curve exhibited for 60 nm gold and S protein mixture was not fully explained by the Boltzmann model shown in Eq. (2). (Fig. 3a). Instead of smooth sigmoidal feature, almost letter "Z"-shape feature was observed. In order to extract out the trend, the data points shown in red (Fig. 3b) were removed from the fit to extract the parameters shown in Table 1a. On the other hand, the plot of $\overline{\lambda_{peak}}$ *vs.* added number of moles of H_3O^+, $n(H_3O^+)$, clearly showed a regular sigmoidal feature and the number of moles of H_3O^+ at the inflection point, $n_o(H_3O^+)$, was extracted with Boltzmann model as shown in Eq. (2) by replacing pH with $n(H_3O^+)$. The pH value at $n_o(H_3O^+)$ matched with $\mathrm{pH_o}$ shown in Table 1a within pH ± 0.07. Two potential explanations are considered for this "Z"-shape feature, one is an ignorance of dynamic factor in our measurement methodology. Since the addition of the acid was continuously conducted with a certain interval, all points have almost an equal time interval (roughly 4 min). The initial data point start showing "Z"-shape feature could contain unresolved dynamics or kinetic pathways resulting in a buffering effect resulting in a slow response of pH change. A second possible explanation is that the pH condition of those removed data points (shown in red in Fig. 3b), which is from 4.21 to 4.05 as well as from 4.08 to 4.10 may correspond to a "trigger" pH values to cause major conformational change especially in S1 protein adsorbed at 60 nm gold colloid. Since 60 nm gold colloid was found to have very low Θ and abnormal features took place before the completion of the gold aggregates formation, the lying-down orientation was formed initially and rearranging to the spiking-out orientation as acid was inserted. In any cases, it may contain some implication of that particular nano-size has some cell biological significance considering that typical size of SARS-CoV-2 was reported to be ~100 nm in diameter [44] and S protein has the length of approximately 18 nm [42,43] (*i.e.,* length of core membrane of SARS-CoV-2 ≈ 100–18 × 2 = 64 nm).

The existence of any reversible processes for S protein mixed with gold nano-particles were examined by pH hopping scheme. We presume that, at the higher pH (pH ~10) and the neutral condition, the gold colloids exist as a dispersed situation presenting the $\overline{\lambda_{peak}}$ ~580 nm. For example, $\overline{\lambda_{peak}}$ = 584(1) nm with three components, λ_i, (and coefficients a_i) defined in Eq. (1); λ_1 = 519.1(1) nm (a_1 = 0.73(1)), λ_2 = 613(2) nm

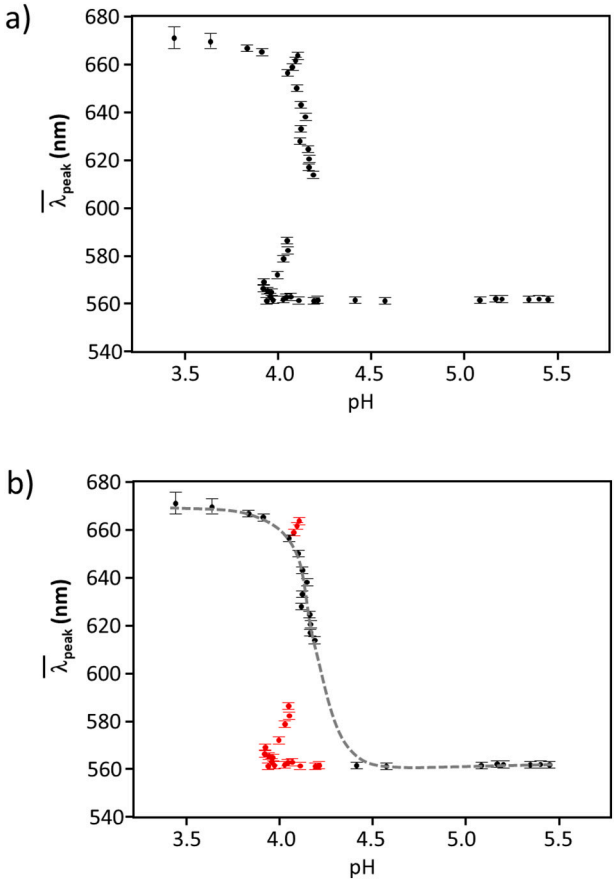

Fig. 3. a) Peculiar sigmoidal feature for 60 nm gold colloid coated with S protein. All data points are shown. b) Peculiar sigmoidal feature for 60 nm gold colloid coated with S protein. The red points which show peculiar behaviors were removed from the fit for Boltzmann model given in Eq. (2). (For interpretation of the references to color in this figure legend, the reader is referred to the web version of this article.)

(a_2 = 0.04(1)), and λ_3 = 786.2(5) nm (a_3 = 0.23(1)) for 10 nm gold with S protein mixture at pH = 6.30(5) [45]. At this pH, regardless of if it is adsorbed to the gold surface or not, the S protein is at the *non-primed* condition and is considered to be close to a native state. On the other hand, at the lower pH (*ca.* pH ~3) the $\overline{\lambda_{peak}}$ red-shifted. For example, $\overline{\lambda_{peak}}$ was around 643(3) nm for 10 nm gold colloid – S protein mixture, λ_1 = 539(5) nm (a_1 = 0.36(5)), λ_2 = 626(11) nm (a_2 = 0.32(2)), and λ_3 = 775.6(6) nm (a_3 = 0.32(4) for pH ~3, and more red-shift was observed as the colloidal size increased. For 100 nm gold colloid with S protein at pH –3, $\overline{\lambda_{peak}}$ was 702.5(6), where λ_1 = 593.7(6) nm (a_1 = 0.42 (1)) and λ_2 = 782.0(6) nm (a_2 = 0.58(1)). For an overall pH range between pH 2 and pH 10, the relatively high stability of S protein mediated gold colloid aggregates was confirmed within the time window of spectrum measurements. However, for the pH < 4, the gold colloid aggregates showed less stability, exhibiting a decrease in absorbance and reaching to a transparent color with precipitation after five or six hours. The acidic condition may further favor aggregates until it results in a precipitate. The kinetic investigation of the aggregation at the longer time window is planned for future work, but at the timescales used in this study nanoparticle aggregation is not a concern.

Based on the studies conducted on amyloidogenic peptides, the red-shift of SPR band suggests the formation of the gold colloid aggregates mediated by the adsorbed proteins [31]. The control study for the aggregation with only bare gold colloid was conducted by both spectroscopic and TEM image [45]. The aggregation (or destabilization) of bare gold colloid takes place at the pH < $\mathrm{pH_o}$. The $\mathrm{pH_o}$ of the bare gold colloid

(10 nm – 100 nm) ranged between 3.0 and 4.2 (see Table 1b). However, no reversible aggregation was observed for bare gold colloid once they were exposed to the acidic condition [45]. Thus the D parameter in Eq. (3) can be an indicator for the adsorption of an S protein.

The status and trend of the change in $\overline{\lambda_{peak}}$, $\Delta\overline{\lambda_{peak}}$, for $n = 1$–20 is summarized in Fig. 4. The quasi-repetition of $\overline{\lambda_{peak}}$ between two distinctly separated values implies the reproduction of reversible process. The pH operation number, n, dependent $\overline{\lambda_{peak}}$ was fit by the analytical formula [46] given in Eq. (3).

$$\overline{\lambda_{peak}}(n) = A + B(n-1)^C + De^{(n-1)E}cos(n\pi) \quad (3)$$

where n indicates the operation of pH change (n = 1, 2, 3, …, 18, 19, and 20). An initial peak position at neutral pH (*i.e.,* $\overline{\lambda_{peak}}$(n = 1)) is given by $A - D$, and the parameters B and C show the average wave peak position shift as pH varies between pH ~3 and pH ~10. The parameters D represents amplitude and E is an amplifying factor (E > 0) or a damping factor (E < 0) for the repetitive undulation expressed by the cosine function. The optimized parameters are listed in Table 2. A clear nano-size dependence was found in the amplitude of undulation, parameter D. For the gold colloid size over 30 nm, D parameter was significantly large. As far as D parameter was focused, the 40 nm gold colloid can support the largest amplitude among studied gold colloids. For the cases of d = 30, 40, 50, and 60 nm gold colloid and S protein mixture, the $\overline{\lambda_{peak}}(n = 2)$ possessed relatively larger standard error meaning that first induction to the lower pH state can be kinetically unstable. The gold colloid of d = 30, 40, and 50 nm had two regions of different D parameters. For example, as for d = 50 nm S protein mixture showed a discontinuity in amplitude between $n = 10$ and 11. There was a clear discontinuity in a repetitive trend for d = 40 nm (between $n = 8$ and $n = 9$), 50 nm (between (n = 10 and $n = 11$), and 60 nm (between n = 8 and 9). Focusing the parameters D and E, D reduced by more than 50% and E significantly reduced at the transition for 40 nm and 50 nm. On the other hand, for 60 nm, D parameter increased and E parameter flipped sign from negative to positive [42]. Comparing the average D values (*i.e.,* $\overline{D} = 14(11)$) and the average E values ($\overline{E} = 0.03(4)$) parameter of gold nano-particle —S protein mixture with those of $A\beta_{1\text{-}40}$ coated 20 nm gold colloid (D = 10 (1) and E = −0.07(2)) the more amplitude and more amplifying trends were noticed. The ovalbumin coated gold nano particles possessed slightly higher amplitude ($\overline{D}$ = 20(8)) and more damping factor ($\overline{E}$ = −0.04(3)) [32].

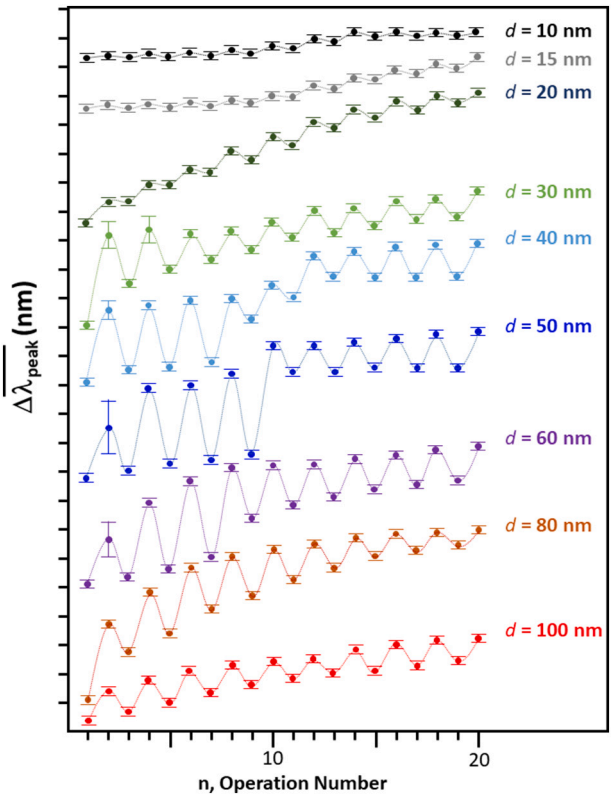

Fig. 4. The trend of shift in SPR band, $\Delta\overline{\lambda_{peak}}$, for tested colloidal particles in this study. (pH ~7 for $n = 1$, pH ~10 for odd n, and pH ~3 for even n).

Table 2
The optimized parameters for the $\overline{\lambda_{peak}}$(n) responses to the pH hopping using the analytical formula shown in Eq. (3) for a mixture of S protein and gold nano-particle of size d at 25 ± 0.5 °C.

d (nm)	A (nm)	B (nm)	C	D (nm)	E	$<R^2>$
10	580(1)	0.7(5)	1.1(2)	1.2(9)	0.002(70)	0.929
15	581(1)	0.16(6)	1.8(1)	1.0(5)	−0.05(4)	0.988
20	583(3)	11(2)	0.72(5)	3(1)	−0.008(33)	0.992
30	593(4)	15(3)	0.48(6)	21(2)	0.09(2)	0.982
40	596(10)	6(6)	0.9(3)	30(7)	0.06(3)	0.898
50	590(12)	8(7)	0.8(3)	26(7)	0.05(3)	0.889
60	574(8)	11(6)	0.7(1)	23(4)	0.04(2)	0.948
80	592(5)	28(4)	0.45(4)	19(3)	0.06(2)	0.985
100	635(1)	5.5(8)	0.70(4)	8.6(6)	0.016(7)	0.995
Average	592(18)	10(9)	0.9(4)	14(11)	0.03 (4)	0.989(7)

In the study of the amyloidogenic coated gold colloid, the sensitivity of the binding affinity was reflected on to the ΔpH_o [30]. However, the ΔpH_o value was a poor measure for the binding affinity of the S protein to the gold surface. For example, S protein coated 40 nm or 60 nm gold had the $\Delta pH_o \sim 0$ (Table 1c). A significant reversible self-assembly was observed for those gold colloids (Fig. 4). Since the reversible self-assembly was attributed to the conformational change of an S protein bound to the gold surface, the sensitivity of the affinity for an S protein may be represented by the D factor (*i.e.*, amplitude factor of reversibility) in Eq. (3). Based on the D values (Shown in Table 2),the larger the colloid size the greater the affinity.

Although beyond the scope of the present work, it is unclear why ΔpH_o is not a good indicator of binding affinity for S protein case. One possibility is that the surface of the S protein may be exhibiting a similar partial negative condition to the gold surface. We are working on quantifying the sensitivity of the SPR band for the attachment by measuring the threshold concentration (C_o) required to cause the nanoparticle protein system aggregation *(e.g.,* $C_o = 1375 \pm 90$ pmol 20 nm gold coated β2m, but $C_o = 40 \pm 28$ pmol for β2m coated 80 nm.) [47] This example exhibits the sensitivity of peptide attachment and resulting networking with a different protein system, and we are hoping to extend this technique to the S protein case.

We reported that the adsorption was due to a charge-dipole interaction between $-N^+H_3$ of the 28th Lysine (^{28}K) and the partially negative gold surface [31]. Similarly, the most plausible interaction between gold surface and S protein is speculated to be a charge-dipole interaction between $-NH^+$ in imidazole ring of the eight series of Histidine (^{1250}H —^{1257}H), which are located in the cytoplasmic domain (1237–1273) [48]. Since an existence of hydrogen bonding between a hydroxyl group and gold (OH-Au) was pointed out as a major interaction at the protein-gold interface [49,50], the binding to the gold surface should be recognized as a relatively strong interaction. Thus, the segment of the S protein responsible for the binding to the gold surface must be least affected by an external pH change, whereas the residual segments conducts folding or unfolding conformational change.

The entire cell fusion process due to primed S protein is summarized in the top red box of Fig. 5a [51–53]. The SARS-CoV-2 is a membrane virus and possesses the lipid bilayers, which are indicated with light brown color. The major process to the cell fusion contains the drastic conformational change of the S protein in the cell-fusion process summarized as seven steps. They are: (i) Up or Down conformation of RBD, (ii) Up conformation RBD binding with ACE2, (iii) the priming event or

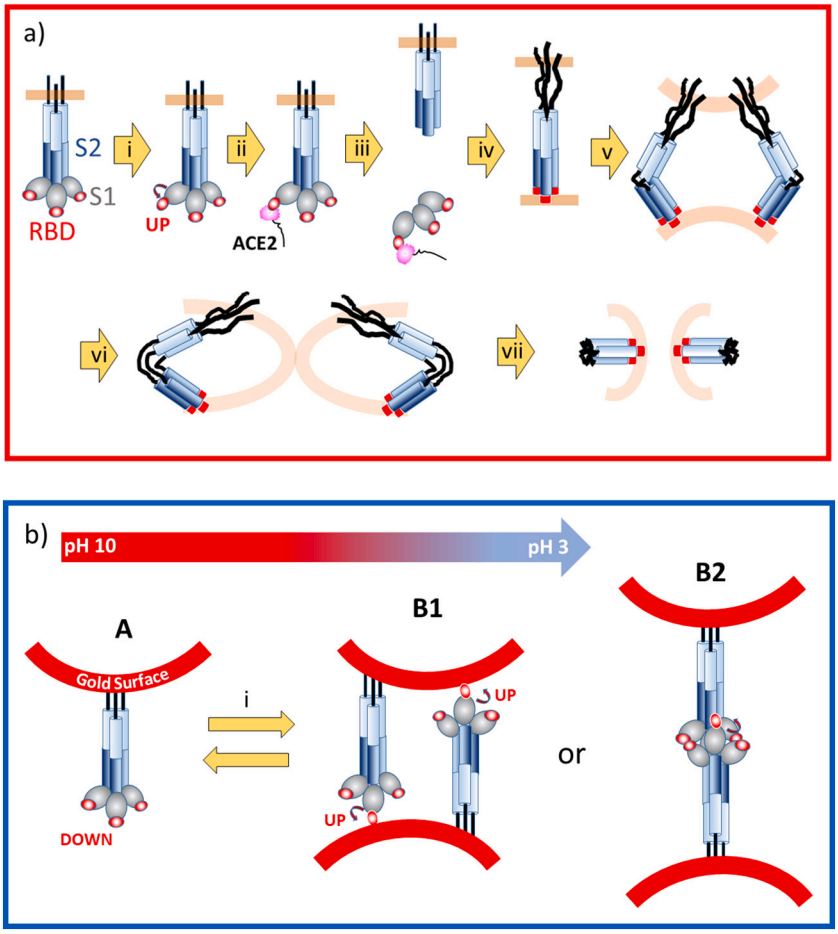

Fig. 5. a) Sketch showing the pre- to post-fusion transition of SARS-CoV-2 S protein. The lipid bilayers are shown with light brown color. (i) Up or Down conformation of RBD, (ii) Up conformation RBD binding with ACE2, (iii) Priming event or trigger, *i.e.,* cleavage of RBD, (iv) formation of pre-hairpin extension of fusion proteins (shown by small red discs at the end of the chain), (v) pre-bundle (close apposition) fold-back, (vi) bundle, *i.e.,* hemifusion, and (vii) fusion. b) Estimated S protein conformational change observed in the current study over the nano-gold colloidal surface. The reversible process may correspond to either Down to Up conformational change of RBD (B1) or dimerization processes of S1 trimers (B2). The structural change of S protein in gradual pH change are estimated with the guidance the arrow indicating the pH change at the top. The conformational change at pH-hopping is estimated as a quasi-reversible process between state A and B at the process (i). (For interpretation of the references to color in this figure legend, the reader is referred to the web version of this article.)

trigger event at the lower pH, where cleavage of the RBD (receptor binding domain) takes place, (iv) the formation of pre-hairpin by an extension of trimers (*protomers*) of fusion proteins by protease under pH ~ 4 and here the hydrophobic segments of fusion proteins attached to the target membrane are shown by small red discs at the end of the chain, (v) the close apposition by the pre-bundle of fusion proteins to cause fold-back which reduces the distance separating the two membranes (~10 Å), (vi) the tight folding of bundle of fusion proteins causes hemifusion of two membranes, and (vii) a completion of the fusion of two cell membranes becoming one bilayer. Considering that bundling the unbundled proteins are expected to be energetically down-hill, all processes must be non-reversible.

The non-zero ΔpH_o and quasi-reversible SPR band peak shift allowed us to estimate adsorption of the S protein over the nano-gold surface especially for those over d = 30 nm, however the coverage ratio was relatively low [30]. Based on the previous studies of amyloidogenic peptide coated gold nano-particles, the drastic red-shift of SPR is considered to be due to the formation of gold colloid aggregates [45]. The formation of aggregates must be mediated by the bonding of S protein adsorbed over the nano-gold surface as shown in Fig. 5b with hydrophobic segments of C-terminal. Because no receptor nor enzymes are present, no critical cell fusion process shown in Fig. 5a, should have been observed in this work. At pH ~10, the RBD portion of S1 may take Down conformation (State A) which is not active for binding to the receptor. At pH ~3, the formation of Up conformation (State B1) of one of the RBD in trimer of S1 or RBD accessing to the other gold colloid surface and resulting in the aggregates formation. Another possibility will be that RBD segment (at either Up or Down confirmation) dimerize and causes gold colloid aggregates (B2). In the gradual pH change, the conformational change between state A and B1 or B2 take place following the pH change arrow shown at the top of Fig. 5b. For pH hopping experiment, a transition between state A and State B1 or B2 may occur as pH hops between pH ~10 and pH ~3.

These results demonstrate that gold nano-particles can be used to study reversible conformational changes in the S protein using SPR band of nano-gold colloid, and that the pH-dependent red-shift shows a particle size dependence. Based on these data, future studies may now be able to elucidate the kinetics of the S protein conformational intermediate states. In addition, the pH hopping technique described herein could be readily adapted for use *in vitro* screening of compounds that alter S protein conformational flexibility or conformational dynamics to support SARS-CoV-2 infection inhibitor discovery efforts.

Declaration of Competing Interest

None.

Acknowledgment

This work was supported by the Geneseo Foundation. A. I. thanks for Gerry Rhodes Scholarship and Kenny Lipkowitz Scholarship. K.Y. appreciates for valuable comments provided by Dr. Jonathan Bourne.

Author statements

Kazushige Yokoyama was responsible for conceptualization, data curation, formal analysis, funding acquisition, methodology, project administration, resources, supervision, validation, visualization, writing-original draft, and writing – review & editing.

Akane Ichiki was responsible for data curation, formal analysis,

methodology, resources, and writing – review & editing.

References

[1] N. Banerjee, S. Mukhopadhyay, Viral glycoproteins: biological role and application in diagnosis, VirusDis. 27 (2016) 1–11.
[2] J.K. Millet, G.R. Whittaker, Physiological and molecular triggers for SARS-CoV membrane fusion and entry into host cells, Virology 517 (2018) 3–8.
[3] M. Yuan, et al., A highly conserved cryptic epitope in the receptor binding domains of SARS-CoV-2 and SARS-CoV, Science 368 (2020) 630–633.
[4] W.C. Hwang, et al., Structural basis of neutralization by a human anti-severe acute respiratory syndrome spike protein antibody, 80R, J. Biol. Chem. 281 (2006) 34610–34616.
[5] J.E. Pak, et al., Structural insights into immune recognition of the severe acute respiratory syndrome coronavirus S protein receptor binding domain, J. Mol. Biol. 388 (2009) 815–823.
[6] M. Donoghue, et al., A Novel Angiotensin-Converting Enzyme–Related Carboxypeptidase (ACE2) converts angiotensin I to angiotensin 1–9, Circulation Research (2000) 1–9.
[7] R. Yan, et al., Structural basis for the recognition of SARS-CoV-2 by full-length human ACE2, Science 367 (2020) 1444–1448.
[8] P. Verdecchia, G. Reboldi, C. Cavallini, G. Mazzotta, F. Angeli, ACE-inibitori, sartani e sindrome respiratoria acuta da coronavirus 2, G. Ital. Cardiol. 21 (2020) 321–327.
[9] A.J. Turner, S.R. Tipnis, J.L. Guy, G.I. Rice, N.M. Hooper, ACEH/ACE2 is a novel mammalian metallocarboxypeptidase and a homologue of angiotensin-converting enzyme insensitive to ACE inhibitors, Can. J. Physiol. Pharmacol. 80 (2002) 346–353.
[10] M. Hoffmann, et al., SARS-CoV-2 cell entry depends on ACE2 and TMPRSS2 and is blocked by a clinically proven protease inhibitor, Cell 181 (2020) 271–280.
[11] C. Vickers, et al., Hydrolysis of biological peptides by human angiotensin-converting enzyme-related carboxypeptidase, J. Biol. Chem. 277 (2002) 14838–14843.
[12] Katovich, M.J., Grobe, J.L., Huentelman, M. & Raizada, M.K. Angiotensin-converting enzyme 2 as a novel target for gene therapy for hypertension. Exp. Physiol. 90, 299–305.
[13] S.R. Tipnis, et al., A human homolog of angiotensin-converting enzyme, cloning and functional expression as a captoril-insensitive carboxypeptidase, J. Biol. Chem. 275 (2000) 33238–33243.
[14] A. Choudhury, S. Mukherjee, In silico studies on the comparative characterization of the interactions of SARS-CoV-2 spike glycoprotein with ACE-2 receptor homologs and human TLRs, J. Med. Virol. (2020) 1–9.
[15] A. Hussaina, et al., Targeting SARS-CoV2 spike protein receptor binding domain by therapeutic antibodies, Biomed. Pharmacother. 130 (2020).
[16] I.S. Kim, et al., Mechanism of membrane fusion induced by vesicular stomatitis virus G protein, PNAS (2016) E28–E36.
[17] D. Wrapp, et al., Cryo-EM structure of the 2019-nCoV spike in the prefusion conformation, Science 367 (2020) 1260–1263.
[18] S. Kang, et al., Crystal structure of SARS-CoV-2 nucleocapsid protein RNA binding domain reveals potential unique drug targeting sites, Acta Pharm. Sin. B 10 (2020) 1228–1238.
[19] Y.A. Malik, Properties of coronavirus and SARS-CoV-2, Malaysian J. Pathol. 42 (2020) 3–11.
[20] A.C. Walls, et al., Structure, function, and antigenicity of the SARSCoV-2 spike glycoprotein, Cell 180 (2020) 281–292.
[21] X. Ou, et al., Characterization of spike glycoprotein of SARS-CoV-2 on virus entry and its immune cross-reactivity with SARS-CoV, Nat. Commun. 11 (2020) 1–12.
[22] W. Tai, et al., Characterization of the receptor-binding domain (RBD) of 2019 novel coronavirus: implication for development of RBD protein as a viral attachment inhibitor and vaccine, Cell. Mol. Immunol. 17 (2020) 613–620.
[23] B. Qiao, & Olvera de la Cruz, M. enhanced binding of SARS-CoV-2 spike protein to receptor by distal polybasic cleavage sites, ACS Nano 14 (2020) 10616–10623.
[24] H. Jiandong, et al., Neutralization of SARS-CoV-2 by destruction of the prefusion spike, Cell Host Microbe 28 (2020) 1–10.
[25] I. Mercurio, V. Tragni, F. Busto, A. De Grassi, C.L. Pierri, Protein structure analysis of the interactions between SARS-CoV-2 spike protein and the human ACE2 receptor: from conformational changes to novel neutralizing antibodies, Cell. Mol. Life Sci. (2020) 1–22, https://doi.org/10.1007/s00018-00020-03580-00011.
[26] R. Alexpandi, J.F. De Mesquita, S.K. Pandian, A.V. Ravi, Quinolines-based SARS-CoV-2 3CLpro and RdRp inhibitors and spike-RBD-ACE2 inhibitor for drug-repurposing against COVID-19: an in silico analysis, Front. Microbiol. 11 (2020) 1–15.
[27] A. Basit, T. Ali, S.U. Rehman, Truncated human angiotensin converting enzyme 2; a potential inhibitor of SARS-CoV-2 spike glycoprotein and potent COVID-19 therapeutic agent, J. Biomol. Struct. Dyn. (2020) 1–10, https://doi.org/10.1080/07391102.07392020.01768150.
[28] A. Bekdemir, S. Liao, F. Stellacci, On the effect of ligand shell heterogeneity on nanoparticle/protein binding thermodynamics, Colloids Surf. B: Biointerfaces 174 (2019) 367–373.
[29] S. Sabella, et al., A general mechanism for intracellular toxicity of metal-containing nanoparticles, Nanoscale 6 (2014) 7052–7061.
[30] K. Yokoyama, A. Ichiki, Oligomerization and adsorption orientation of amyloidogenic peptides over nano-gold colloidal particle surfaces, in: J.C. Taylor (Ed.), Advances in Chemical Research vol. 61, NOVA Science Publisher, Hauppauge, NY, USA, 2020, pp. 139–194.
[31] K. Yokoyama, et al., Examination of adsorption orientation of amyloidogenic peptides over nano-gold colloidal particles' surfaces, Int. J. Mol. Sci. 20 (2019) 5354–5380.
[32] K. Yokoyama, et al., Nanoscale size dependence in the conjugation of amyloid beta and ovalbumin proteins on the surface of gold colloidal particles, Nanotechnology 19 (2008) 375101–375108.
[33] Q. Zhang, et al., Cellular nanosponges inhibit SARS-CoV-2 infectivity, Nano Lett. 20 (2020) 5570–5574.
[34] L. Rao, R. Tian, X. Chen, Cell-membrane-mimicking nanodecoys against infectious diseases, ACS Nano 14 (2020) 2569–2574.
[35] K. Kalantar-Zadeh, S.A. Ward, K. Kalantar-Zadeh, E.M. El-Omar, Considering the effects of microbiome and diet on SARS-CoV-2 infection: nanotechnology roles, ACS Nano 14 (2020) 9202–9205.
[36] M.C. Sportelli, et al., Can nanotechnology and materials science help the fight against SARS-CoV-2, Nanomaterials 10 (2020) 802–813.
[37] G. Reina, S. Peng, L. Jacquemin, A.F. Andrade, A. Bianco, Hard nanomaterials in time of viral pandemics, ACS Nano 14 (2020) (9364-0388).
[38] D.S. Chauhan, et al., Comprehensive review on current interventions, diagnostics, and nanotechnology perspectives against SARS-CoV-2, Bioconjug. Chem. 31 (2020) 2021–2045.
[39] H. Sekimukai, et al., Gold nanoparticle-adjuvanted S protein induces a strong antigen-specific IgG response against severe acute respiratory syndrome-related coronavirus infection, but fails to induce protective antibodies and limit eosinophilic infiltration in lungs, Microbiol. Immunol. 64 (2019) 33–51.
[40] K. Gorshkov, et al., Quantum-dot-conjugated SARS-CoV-2 spike pseudo-virions enable tracking of angiotensin converting enzyme 2 binding and endocytosis, ACS Nano 14 (2020) 12234–12247.
[41] R. Ling, et al., In silico design of antiviral peptides targeting the spike protein of SARS-CoV-2, Peptides 130 (2020) 1–7.
[42] Yokoyama, K. & Ichiki, A. Nano-size dependence in the adsorption by the SARS-CoV-2 spike protein over gold colloid. Colloid and Surfaces A (under the review).
[43] D. Wrapp, et al., Structural basis for potent neutralization of betacoronaviruses by single-domain camelid antibodies, Cell 181 (2020) 1004–1015.
[44] Y.M. Bar-On, A. Flamholz, R. Phillips, R. Milo, SARS-CoV-2 (COVID-19) by the numbers, eLife x 9 (2020) 1–15.
[45] K. Yokoyama, et al., Microscopic investigation of reversible nanoscale surface size dependent protein conjugation, Int. J. Mol.Sci. 10 (2009) 2348–2366.
[46] K. Yokoyama, D.R. Welchons, The conjugation of amyloid beta protein on the gold colloidal nanoparticles' surfaces, Nanotechnology 18 (2007) 105101–105107.
[47] K. Yokoyama, et al., Modeling of the aggregation process of beta 2 microglobulin coated nano-gold colloids, in preparation, 2020.
[48] H. Woo, et al., Developing a fully glycosylated full-length SARS-CoV-2 spike protein model in a viral membrane, J. Phys. Chem. B 124 (2020) 7128–7137.
[49] J. Torsten, et al., Impact of nanoparticles on amyloid peptide and protein aggregation: a review with a focus on gold nanoparticles, Nanoscale 10 (2018) 20873–21536.
[50] S. Rai, N.S. Kumar, H. Singh, A theoretical study on interaction of proline with gold cluster, Bull. Mater. Sci. 35 (2012) 291–295.
[51] J. Shanga, et al., Cell entry mechanisms of SARS-CoV-2, in: PNAS Latest Articles, 2020, pp. 1–8.
[52] W. Song, M. Gui, X. Wang, Y. Xiang, Cryo-EM structure of the SARS coronavirus spike glycoprotein in complex with its host cell receptor ACE2, PLOS Pathog. (2018) 1–19.
[53] J.M. White, G.R. Whittaker, Fusion of enveloped viruses in endosomes, Traffic 17 (2016) 593–614.